

12.2 Improving the Range of WiFi Backscatter Via a Passive Retro-Reflective Single-Side-Band-Modulating MIMO Array and Non-Absorbing Termination

Miao Meng¹, Manideep Dunna¹, Hans Yu¹, Shihkai Kuo¹, P-H. P. Wang^{1,2}, Dinesh Bharadia¹, Patrick P. Mercier¹

¹University of California San Diego, La Jolla, CA

²Broadcom, San Diego, CA

Wi-Fi is the most ubiquitous wireless networking technology for IoT in homes, offices, and businesses. Since the power of Wi-Fi transceivers (10s-to-100s of mW) can be prohibitively high for emerging classes of IoT devices (which desire <100 μ W), recent work has suggested piggybacking baseband signals from the IoT device directly on top of incident Wi-Fi signals generated by access points (APs) via Wi-Fi-compatible backscatter modulation [1-4], where as low as 28 μ W of active power has been demonstrated [4]. However, the major limitation of this approach is range: signals generated by the transmitting AP experience $1/d^2$ path loss to the backscattering tag, which has insertion loss $P_{L,ins}$ to perform single-side band (SSB) modulation, and then re-radiated modulated signals back to the receiving AP (or to another AP) experience an additional $1/d^2$ path loss, resulting in an overall loss $\propto 1/d^4 + P_{L,ins}$. With no active RF amplification, the tag in [4] experienced $P_{L,ins}=15$ dB, limiting AP-to-tag-and-back-to-AP distance to ~ 10 m, which is not sufficient in many single-AP homes.

To increase range over state-of-the-art, this paper proposes a design that improves the only parameter not currently limited by physics in a single antenna solution: $P_{L,ins}$. In applications where there is sufficient area for multiple antennas, a second design is also proposed that utilizes a passive MIMO-based approach. Specifically, these two designs are fabricated in a single Wi-Fi-compatible IC that employs: 1) a non-absorbing termination approach that enables fully-reflective SSB backscatter modulation, improving measured gain by 4dB and range to 13m; and 2) an entirely passive MIMO antenna array that steers a directional beam back to the AP in a retro-reflective manner while maintaining SSB operation via an IQ-modulated Van Atta array, improving measured gain by 15dB and range to 23m towards pragmatic adoption in home and office environments.

Figure 12.2.1 illustrates the approach in [4] in contrast to the two proposed approaches. In [4] (top left), incident Wi-Fi signals at one channel (e.g., Ch 6) pass through a power splitter, and the top IQ path encounters either an absorbing 50 Ω termination (reflection coefficient $\Gamma = 0$), or a reflecting open circuit ($\Gamma = e^{j\pi}$), depending on the IF clock and the I BB data. Similarly, the bottom IQ path encounters either a reflection ($|\Gamma| = 1$ by setting $C=1.2$ pF at 2.4GHz to make $\Gamma = e^{j\pi-90^\circ}$), or 50 Ω . The resulting reflected IQ signals combine to re-radiate a SSB QPSK-modulated signal at another Wi-Fi channel (e.g., Ch 1 or 11), for reception by either a single dual-radio AP, or a different AP located elsewhere. This approach results in a signal that is only reflected part of the time, resulting in additional losses that are not theoretically required.

The first proposed solution, shown in Fig. 12.2.1 (bottom right), is to always present a reflecting load, for example by replacing the 50 Ω terminations with either a short ($\Gamma = e^{j\pi-180^\circ}$) or a positive reactance ($\Gamma = e^{j\pi-90^\circ}$). This approach retains the ability to generate SSB QPSK signals, and theoretically increases the total reflected power simply by adding a 0.7mm² 3.3nH inductor with no additional power cost.

However, this still suffers from a major drawback: reflected power is radiated omnidirectionally, delivering precious re-radiated power away from the desired receiving AP. MIMO is a well-known technique that can help by steering radiated power in a narrow beam targeting the desired receiver. However, despite gains from MIMO techniques being the driving force behind major improvements in nearly all wireless systems over the last two decades, MIMO conventionally requires multiple precision LOs with finely tuned phase delays to enable beam steering, which is completely impractical in a low-power IoT device. For this reason, MIMO has, until now, never been made to work well in passive Wi-Fi backscatter systems.

This work realizes the benefits of MIMO into a Wi-Fi-compatible backscatter system by leveraging the concept of a Van Atta retro-reflector [5], which reflects incident waves back to their source in a fully passive manner. As shown in Fig. 12.2.1 (top right), this technique eliminates the need for a power splitter and enables a self-steered beam with directional gain, thereby significantly extending the range. Fig. 12.2.2 outlines one possible implementation of a modulated Van Atta array (left) in contrast to the proposed approach (right). By properly selecting the delay through the transmission lines connecting each antenna, incident RF signals at angle θ will be re-radiated in a steered

beam back at the same angle. Simply alternating between the re-radiation condition and a 50 Ω terminated condition at the BB data rate could enable OOK backscatter, while mixing the BB with an IF clock would enable PSK backscatter at frequency-shifted channels. However, the generated double sideband signal undesirably occupies all three Wi-Fi channels, and the periodically-absorbing condition reduces the amount of re-radiated power. To overcome these challenges, this work proposes an IQ-modulated Van Atta structure, where 90 $^\circ$ and 180 $^\circ$ transmission-line (TRL)-based delays are intentionally added between antennas to enable QPSK SSB reflections. Specifically, the outer two antennas are connected by a switched pair of 270 $^\circ$ and 90 $^\circ$ TRLs and modulated by a Q-phase IF signal, while the inner two antennas are connected by a switched pair of 0 $^\circ$ and 180 $^\circ$ TRLs (i.e., 90 $^\circ$ separated from the outer antennas) and driven by the I-phase IF signal. This multi-antenna structure improves measured gain by upwards of 15 and 11dB over the prior partially-absorbing and proposed fully-reflective approaches, respectively.

The proposed backscattering tag, whose schematic is shown in Fig. 12.2.3, uses an integrated wake-up receiver (WuRX) that performs energy detection on a pre-specified sequence of packets to synchronize a backscattering event [4]. Since the timing gaps between the packets cannot be guaranteed in a realistic fully-standards-compliant Wi-Fi network, a correlator-based WuRX like in [4], which relies on a specific ON-OFF pattern, is not pragmatic. Instead, a counter-based scheme which measures the length of the packets T0 and T1 is leveraged, which at very limited additional power enables a robust wake-up circuit, which can scale up and be employed to enable operation on even crowded networks.

The proposed backscatter IC was fabricated in 65nm, occupying 0.44mm². Fig. 12.2.4 (top) shows via wired measurements through a 23dB-isolation circulator and 4-way splitter (used for testing purposes only) how incident 802.11b Wi-Fi signals at Ch 6 can be reflected to either channel 1 or 11 (note: the residual signal at Ch 6 is due to finite circulator isolation). Measurements here indicate the MIMO approach improves insertion loss by 15dB over [4] and by 11dB over the fully-reflective approach (which itself improves by 4dB over [4]). Importantly, this does not come at the cost of image rejection, which is still 14-18dB (note: better at Ch 11 due to better TRL matching at that frequency).

During wake-up/synchronization mode, the chip consumes 4.5 μ W, and can successfully wake-up to the desired signatures (Fig. 12.2.4 bottom left) with a sensitivity of -43.5dBm (Fig. 12.2.4 bottom right), which is sufficient for >30m operation in normal office environments [4]. The IC consumes 32 μ W for the fully-reflective approach and 38 μ W for the MIMO approach during active backscattering mode, both dominated by the power of stable clock generation to ensure low carrier frequency offset during channel frequency translation.

Wireless experiments using commercial Wi-Fi hardware shown in Fig. 12.2.5 indicate that the proposed retro-reflective MIMO approach achieves a range of approximately 23m for single-AP networks regardless of the angle between the tag and the AP, in both outdoor and typical indoor office conditions. In applications where the area of an antenna array is impractical, the proposed single-antenna reflective termination approach improves the worst-case D1+D2 (AP1-to-tag-to-AP2) distance between APs in a mesh network from 20m to 26m, which improves the practicality of Wi-Fi backscatter systems for next-generation IoT. In cases where the Wi-Fi source (for example a cellular phone) is within 5m of the tag, communication to an AP >30m away is possible with the single-antenna fully-reflective termination approach. A die micrograph is shown in Fig. 12.2.7.

Acknowledgement:

This work was supported in part by the National Science Foundation under Grant 1923902.

References:

- [1] A. Shirane et al., "A 5.8GHz RF-Powered Transceiver with a 113 μ W 32-QAM Transmitter Employing the IF-based Quadrature Backscattering Technique" *ISSCC*, pp. 248-249, Feb. 2015.
- [2] B. Kellogg et al., "Passive Wi-Fi: bringing low power to Wi-Fi transmissions," in *Proc. of the Conference on Networked Systems Design and Implementation*, pp. 151-164, Mar. 2016.
- [3] P. Zhang et al., "HitchHike: Practical Backscatter Using Commodity WiFi," in *Proc. of the ACM Conference on Embedded Network Sensor Systems*, pp. 259-271, Nov. 2016.
- [4] P.-H. Wang et al., "A 28 μ W IoT Tag that can Communicate with Commodity WiFi Transceivers via a Single-Side-Band QPSK Backscatter Communication Technique," *ISSCC*, pp. 312-313, Feb. 2020.
- [5] L.V. Atta, "Electromagnetic reflector," U.S. patent 514040, 1959.

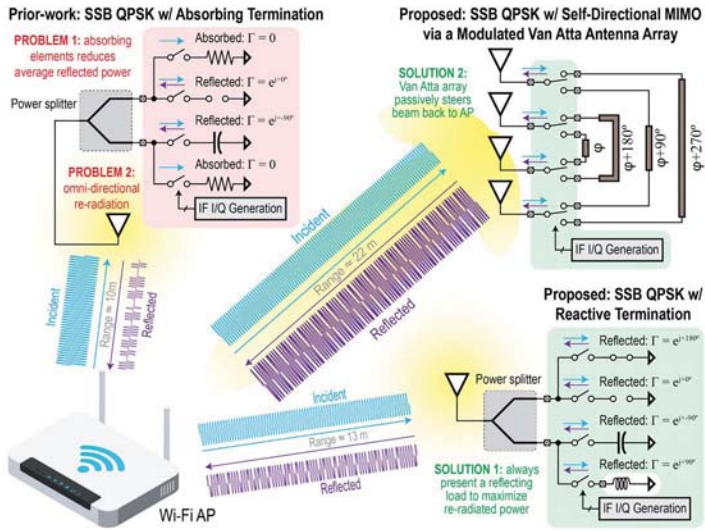


Figure 12.2.1: Overview of prior-art absorbing backscatter (top left), and the proposed approaches using fully reflective termination (lower right) and a passive MIMO approach with SSB modulation (top right).

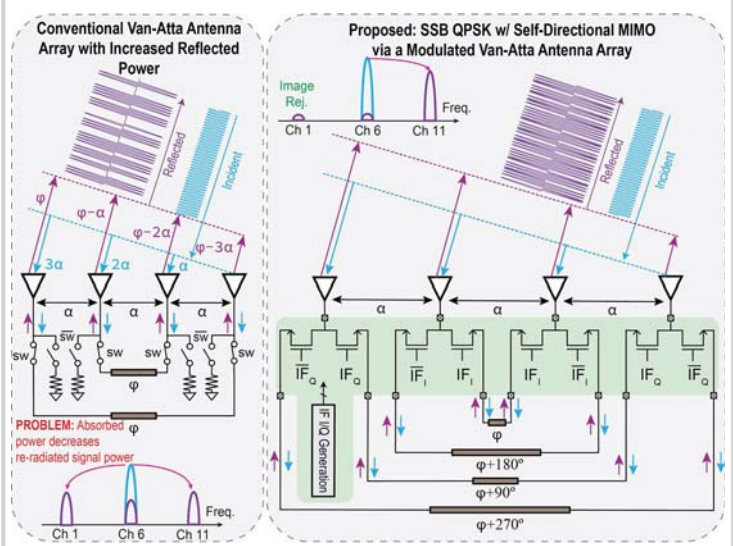


Figure 12.2.2: Approaches to perform Van-Atta array-based backscatter modulation: conventional DSB OOK (left); proposed SSB QPSK approach (right).

12

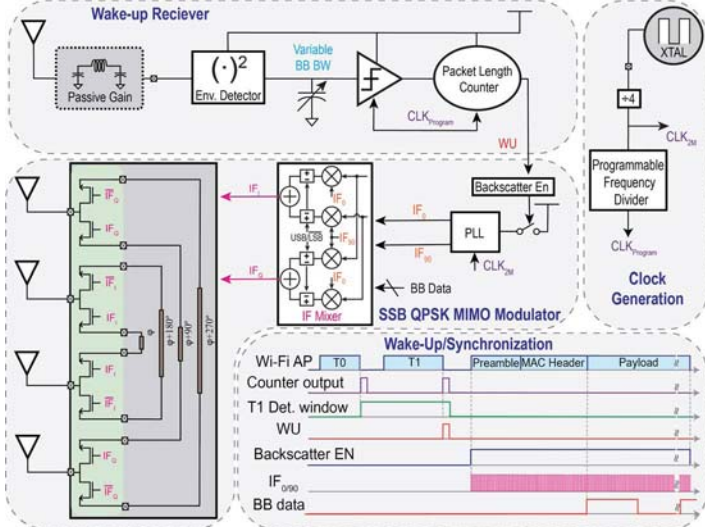


Figure 12.2.3: Block diagram of the proposed backscatter tag with fully WiFi compatible wake-up receivers (top); wake-up/synchronization and backscatter timing (bottom).

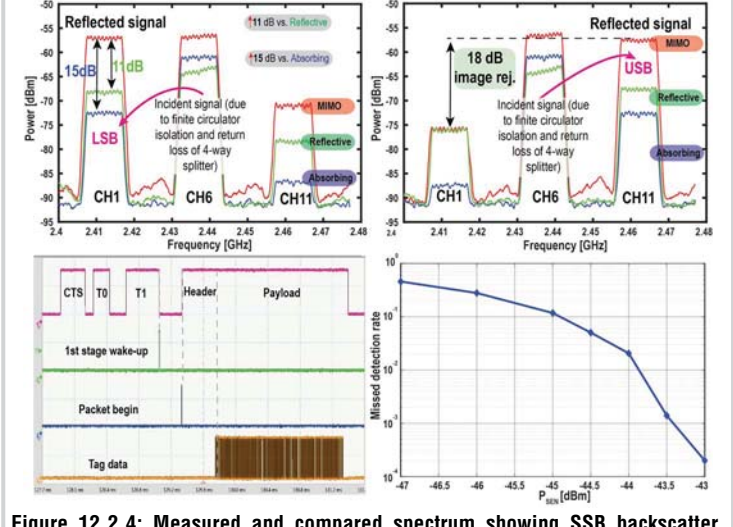


Figure 12.2.4: Measured and compared spectrum showing SSB backscatter frequency translation to lower (top left) and upper (top right) sidebands for all three approaches; measured wake-up and backscatter sequence (bottom left); measured missed detection rate for WuRx (bottom right).

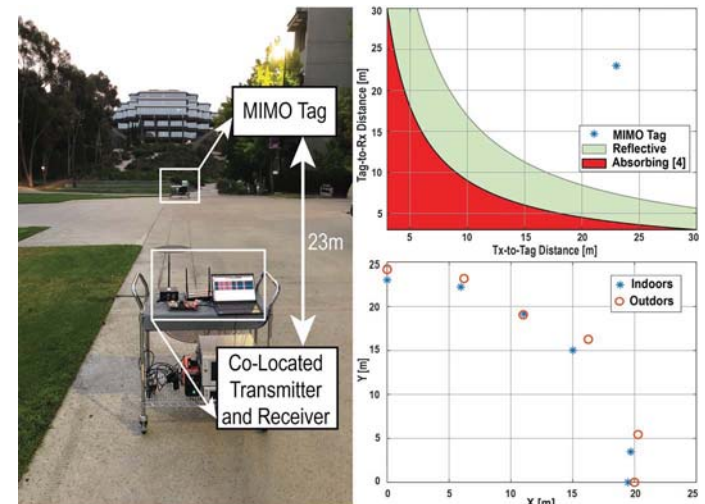


Figure 12.2.5: Wireless experimental setup with co-located Transmitter and Receiver (Left); Maximum range comparison of different variants of backscatter tags (Top Right); Figure demonstrating the retro-reflective nature of MIMO tag (Bottom Right).

| | [1] | [2] | [3] | [4] | This work | |
|--------------------------------------|----------------------------------|--|-----------------------------------|--|---------------------------------------|--|
| | | | | | Fully-Reflective | MIMO |
| Technology (nm) | 65 | NA | NA | 65 | | 65 |
| Chip Size (mm ²) | 0.26 | NA | NA | 0.34 | 0.38 | 0.41 |
| Scheme | Backscatter | Backscatter | SSB WiFi Backscatter | SSB Partially Absorbing WiFi Backscatter | SSB Fully Reflective WiFi Backscatter | SSB Passive Retro-Reflective MIMO WiFi Backscatter |
| Frequency (GHz) | 5.8 | 2.4 | 2.4 | 2.4 | | 2.4 |
| Range: equidistance TX and RX (m) | 0.1 | 4.6 | 6 | 10.5 | 13 | >23 |
| Incident signal source | Tone Transmitter | Tone Transmitter | WiFi | WiFi | | WiFi |
| WiFi Compatibility | Wake-up: No Communication: No | Wake-up: No Communication: Partially* | Wake-up: No Communication: Yes | Wake-up: ~Yes Communication: Yes | Wake-up: Yes Communication: Yes | Wake-up: Yes Communication: Yes |
| Wake-up range (m) | 0.1 | 2.1 (BER = 1e-2) | 6 | >30 | | >30 |
| Wake-up power (µW) | 8.2 | 18 (COTS) | NA | 2.8 | | 4.5 |
| Backscatter communication power (µW) | 113 | 59.2** | 33** | 28 | 32 | 38 |

*WiFi Rx Only

**Simulated

Figure 12.2.6: Comparison table of this work to prior-art.

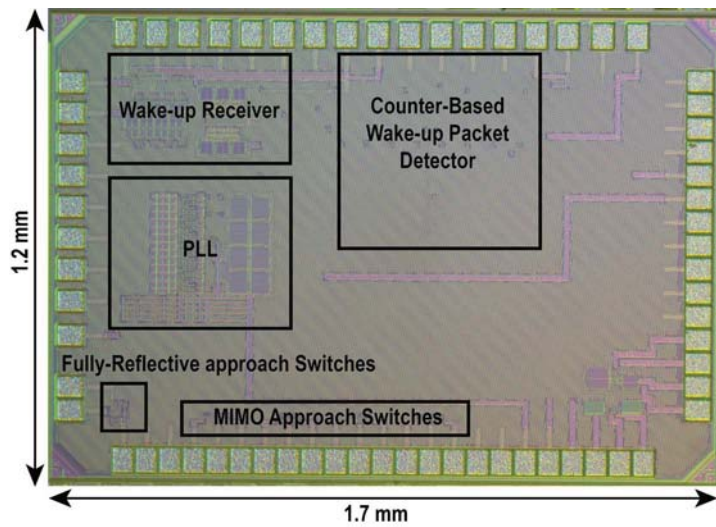


Figure 12.2.7: Micrograph of the chip.